International Journal of Nanotechnology
and Application (IJNA)
ISSN (P): 2277-4777; ISSN (E): 2278-9391
Vol. 7, Issue 3, Dec 2017, 1-16

Original Article

SYNTHESIS AND CHARACTERIZATION OF In_2S_3 NANOPARTICLES BY ELECTROCHEMICAL METHOD: EVALUATION OF ITS PERFORMANCE IN PHOTO-ASSISTED DEGRADATION OF INDIGO CARMINE DYE,ANTIBACTERIAL AND ANTIMITOTIC ACTIVITY STUDIES

HOSAHOLALU BALAKRISHNA UMA[1], SANNAIAH ANANDA[2] & VITTAL RAVISHANKAR RAI [3]

[1,2]*Department of Studies in Chemistry, University of Mysore, Mysuru, India*

[3]*Department of Studies in Microbiology, University of Mysore, Mysuru, India*

ABSTRACT

This article deals with the novel electrochemical synthesis of In_2S_3 nanoparticles, their application in photocatalysis, electrical conductance and biological activity. The synthesized nanoparticles were characterized by XRD, UV-VIS, DLS and FE-SEM (EDAX) techniques. The UV-Visible spectrum revealed that, the synthesized nanoparticles are photoactive under UV light radiation. The X-ray diffraction reveals that, the average crystalline size to be 76.3 nm. The photo catalytic decolorization of the Indigo carmine dye, follows first order reaction. The antimitotic activity has been evaluated, using Allium Cepa by the method of Levan. The antibacterial activity of In_2S_3 nanoparticles, against bioluminescent Photo bacterium lieognathi was investigated.

KEYWORDS: Electrochemical Synthesis, In_2S_3 Nanoparticles, Photo Catalytic Activity, Allium Cepa & Photo Bacterium Lieognathi

Received: Sep 20, 2016; **Accepted:** Oct 12, 2017; **Published:** Oct 28, 2017; **Paper Id.:** IJNADEC20171

INTRODUCTION

Indium Sulfide (In_2S_3) is an important material, for optoelectronic and photovoltaic applications and is a promising candidate, for many technological applications due to its stability, wider band gap and photoconductive behavior. These materials have possible applications in solar cells [1]. Indium sulfide is an III-VI group semiconductor [2], which has important photoluminescence properties [3] and hence, finds larger applications in optoelectronic devices [4]. Indium sulphide has two composite forms of InS and In_2S_3, with band gaps of 2.44 and 2.0 – 2.2 eV, respectively [2]. At atmospheric pressure, In_2S_3 is found to crystallize into three different structural forms, defective cubic structure (α-In_2S_3), defective spinel structure (β-In_2S_3) and layered hexagonal structure (γ-In_2S_3). Among, these three forms β-In_2S_3 has gained much attention, because of its unique electronic [5], optical [6], optoelectronic [7] and semiconductor sensitization [8] properties. Among various inorganic semiconducting materials β-In_2S_3 has been of great interest, because of its quite interesting structure and potential properties. β-In_2S_3 is an n-type semiconductor, with an energy gap between 2.0 and 2.2eV [7, 9]. This has been used as a buffer layer in solar cells [10], a hetero junction in photovoltaic electric generators [11], a photo catalytic material for hydrogen

evolution [12-15], biological image sensors [16] and a photo catalytic material, for degradation of dyes [17,18]. β-In_2S_3 can be used as an effective non- toxic substitute, for CdS in $CuInSe_2$ and $CuInS_2$ based solar cells [19-21]. This material not only eliminates toxic Cadmium, but also improves light transmission, in the blue wavelength region on having band gap, wider than that of CdS. However, the synthesis and potential applications of α-In_2S_3 are rarely reported.

The synthesis of nanostructured electronic materials has been of great interest, to material scientists and chemists due to their various potential applications [22-25]. The preparation of thin films of group III sulfides has been widely reported. In_2S_3 thin film solar cells have been reported with 16.4% efficiency [26]. In_2S_3 dendrites were prepared, via an oxidation and sulphidation growth route [27]. In_2S_3 nanorods were obtained by metal- organic chemical vapour deposition approach [28]. However, synthetic routes to prepare In_2S_3 nanoparticles are scantily reported. Indium sulphide nanoparticles have been reported, by various techniques like solvothermal reduction [29], arrested precipitation techniques [16], sonochemical [30], and hydrothermal methods [4].

In the current paper, we report the synthesis of cubic In_2S_3 nanoparticles by electrochemical procedure, which is achieved by passing an electric current, between two or more electrodes, separated by an electrolyte. By definition the synthesis takes place, at the electrode- electrolyte interface [31, 32]. Some of the advantages of this method are the high purity of the particles and the possibility of the precise particle size (due to decrease in band gap) control, achieved by adjusting the current density. For optimization, it is necessary to take into account the following parameters: the choice of the right solvent, supporting electrolyte, type of electrode and the current density [33]. The catalytic property on photo degradation of Indigo carmine dye and antibacterial activity, using gram negative bioluminescent *photo bacterium leiognathi* and antimitotic activity, using *Allium cepa* have been reported here.

EXPERIMENTAL

Materials

All chemicals used were of analytical grades of purity, Indium (III) Chloride (99.99 % metal base) was purchased from Alfa Aesar, Sodium Sulfide from Alfa-Aesar and Indigo carmine dye from Merck. All solutions were prepared in double distilled water. Optical absorption spectra were recorded at room temperature, on JASCO- UV VIS spectrophotometer. The crystallographic interpretations were performed by X-ray diffractometer (Rigaku miniflex II desktop X-ray diffractometer), using Cu kα wavelength (λ = 1.54 Å). The morphological feature of the semiconductor was observed by scanning electron microscopy (Zeiss Evo LS15). The elemental analysis of the nanoparticles is confirmed, from Energy dispersive X- ray analysis (EDAX), recorded on HITACHI S-3400N JAPAN. Impedance measurement was done using WAYNE KERR 6500B precision impedance analyser.

Electrochemical Synthesis of In_2S_3 Nanoparticles

Nanoscaled In_2S_3 was synthesized, by the electrochemical process using Indium coated platinum electrode in an aqueous system, using sodium sulphide as conductive salt. Sodium sulphide was employed as sulphur source. An electrochemical process based on an electrochemical cell, where M^{n+} coated platinum electrode was used as anode and uncoated pt-electrode, as cathode with lateral distance of 1cm. They were fixed in a holder, so that they were completely enclosed by the electrolyte. A potential difference of 20V was applied between the electrodes, using a DC source. Electrochemical synthesis of In_2S_3 involves two steps. Firstly, Indium is electrochemically deposited, on pt- electrode from an aqueous solution of Indium chloride (0.05M). Secondly, the Indium coated platinum electrode, connected to anode gets

oxidized in Sodium sulphide solution, to yield nanoparticles of In_2S_3. The size of nanoparticles depends on experimental parameters, such as current density, distance between two electrodes and volume of Na_2S solution. The synthesis is optimized to 20ml of Na_2S. The nanoparticles thus, formed was washed repeatedly with distilled water, until sodium sulphide is completely removed, centrifused and calcined, for 2hr to remove sodium and hydroxide impurities, which was formed, due to electrolysis and atmospheric oxidation. High melting point of indium sulphide (1,050^{o}C) affords calcinations to 800^{0}C.

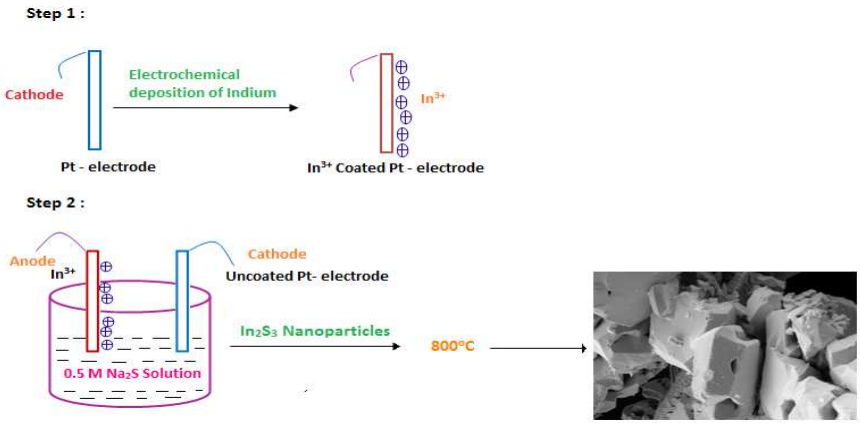

Figure 1: Graphical Representation of Electrochemical Formation of In_2S_3

$$InCl_3 \rightleftharpoons In^{3+} + 3Cl^-$$

$$Na_2S + 2H_2O \rightleftharpoons 2NaOH + S^{2-} + H_2$$

$$2In^{3+} + 3S^{2-} \rightleftharpoons In_2S_3$$

Scheme 1: Mechanism for Synthesis of In_2S_3 Nanoparticles

Determination of Photo catalytic Activities

The photo reactivity of nanocatalysts are influenced by variables, such as the dopant, pH of solution, dosage of photo catalyst, concentration of dye and exposure to different source of light iz. sunlight and UV light [34,35]. Indigo carmine (IC) dye (Molecular formula: $C_{16}H_8O_8N_2S_2$, Molecular weight: 466.16, λ_{max} =610 nm) solution was prepared by dissolving in distilled water (1×10^{-4} M stock solution). This solution was used as test contaminant, for evaluating photo catalytic activities. To assess the photo catalytic efficiency of the prepared nanoparticles, photo degradation experiments were carried out using different concentration of Indigo carmine dye, as substrate and different concentrations of In_2S_3 as catalyst. A calculated amount of catalyst was added to the dye solution, stirred in dark for 1 min to establish adsorption/ desorption equilibrium between dye and nanoparticles, and then illuminated under 8 W UV source to induce a photochemical reaction. Aliquots were taken at an interval of 5 minutes and percent transmittance was determined.

To account for the mineralization of dye Chemical Oxygen Demand (COD), was determined at different stages. The COD was measured according to the standard dichromate titration method [36,37]. The decrease in COD (mg/ L) and increase in % T of the dye solution, with color removal was observed. The formation of different radical species, during photo degradation is given in Scheme 2. The dye was found to have mineralized into H_2O, CO_2 and simpler inorganic salts, after being irradiated using In_2S_3 photo catalyst.

The adsorption and photo catalytic conversion (g %) was calculated as follows [38] :

$$COD = \frac{8000\ (\text{vol of FAS in blank - vol of FAS in dye soln})\ \text{normality of FAS}}{\text{Sample volume}}$$

The photo degradation efficiency of the catalyst was calculated by following Formula

$$\%\ \text{Efficiency} = \frac{\text{Initial COD} - \text{Final COD}}{\text{Initial COD}} \times 100$$

The mechanism of photo degradation can be represented as follows [39, 40]:

$$Np + hv \longrightarrow e^- + h^+$$
$$h^+ + H_2O \longrightarrow OH\cdot + h^+$$
$$h^+ + OH^- \longrightarrow OH\cdot$$
$$e^- + O^2 \longrightarrow O_2^-$$
$$O_2^- + H_2O \longrightarrow HO_2\cdot + OH\cdot$$
$$HO_2\cdot + H_2O \longrightarrow OH\cdot + H_2O$$
$$H_2O_2 \longrightarrow 2OH\cdot$$
$$OH\cdot + IC \longrightarrow \text{Intermediate products}$$
$$\longrightarrow \text{Degradation products}$$
$$O_2^- + IC \longrightarrow \text{Intermediate products}$$
$$\longrightarrow CO_2\ ,\ H_2O\ ,\ NH_3 \text{ and other degradation products}$$

Scheme 2: Mechanism of Dye Degradation by OH Radical

RESULTS AND DISCUSSIONS

X-Ray Diffraction

The XRD pattern of the prepared In_2S_3 nanoparticles is displayed in Figure 2, which exhibits sharp diffraction peaks. The (hkl) values according to Treor programming (IUCR) of the peaks 21.48^0, 30.59^0, 32.92^0, 35.49^0, 37.70^0, 41.84^0, 45.72^0, 49.35^0, 51.04^0, $56.01^{0,}$ 59.13^0, 60.68^0, 62.21^0, 63.67^0 and 68.03^0, corresponds to crystal planes of (211), (222), (222), (400), (330), (332), (510), (521), (440), (611), (541), (622), (631), (444) and (721), respectively. The average crystallite size was calculated using Debye Scherrer equation, which is further confirmed by Williamson – Hall plot [41] and it was found to be 76.3nm, the unit cell volume is 1034.9 $Å^3$ and $\alpha = \beta = \gamma = 90^0$,(a = b= c= 10.11 Å). Accordingly, In_2S_3 belongs to cubic crystal system (α- In_2S_3). The obtained diffraction peaks are well in agreement with that of the reported XRD results, with lattice parameter of a=10.11 Å, which is consistent with the reported value of a= 10.71 Å (JCPDS Card No.65-0459) [42]

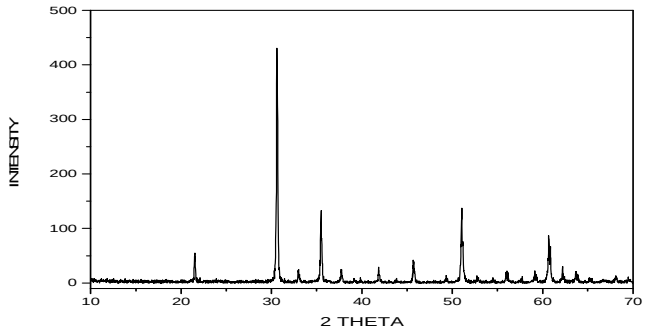

Figure 2: XRD Pattern of In_2S_3 Nanoparticles

Optical Absorption Spectrum and Optical Band Gap

From the optical absorption spectra it is clear that, maximum absorption for In_2S_3 nanoparticles is at 350 nm. This peak position reflects the band gap of this nanoparticle and the synthesized nanoparticles are photoactive, under UV light radiation. There is no absorption peak at visible region. The indirect band gap of the sample is calculated, using Tauc's plot [43,44] by plotting (αhm)$^{1/2}$ verses hγ and then, extrapolating the straight portion of the curve, on *hγ* axis at α=0 as shown in figure 4 and found to be 2.9 eV. This is significantly blue shifted from that of bulk In_2S_3 (λ_{max} = 601nm, E_g = 2.07 eV) and consistent with the quantum confinement effect [45].

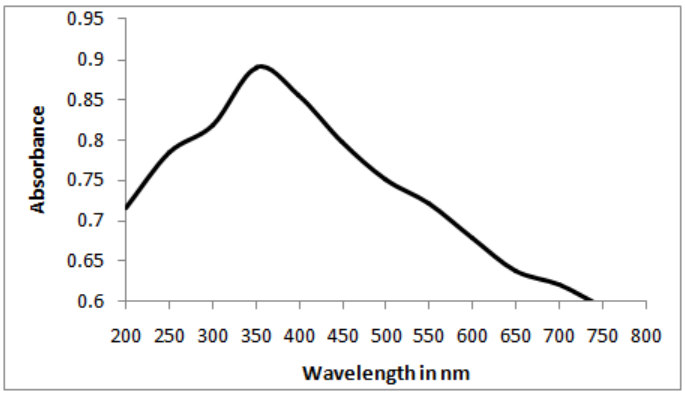

Figure 3: UV-Visible Spectrum of In_2S_3 Nanoparticles

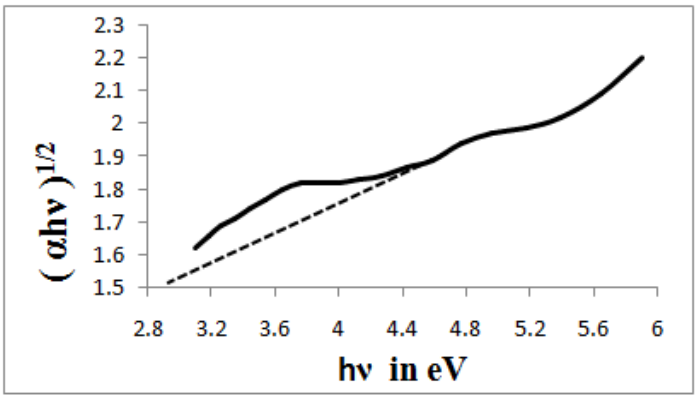

Figure 4: Tauc's Plot of In_2S_3 Nanoparticles

Scanning Electron Microscopy (SEM) and Energy Dispersive X-ray Analysis (EDAX)

The morphology of In_2S_3, Nanoparticles was investigated by FE – SEM shown in Figure 5. The SEM observations can reveal that, the sample consists of aggregates of particles (Figure 5A), with irregular hexagonal cluster (Figure5B) like structure. The elemental analysis of In_2S_3 nanoparticles was carried out using EDAX, to confirm the presence of Indium and Sulphur. The EDAX result also shows the presence of smaller amount of oxygen as impurity (Figure 6).

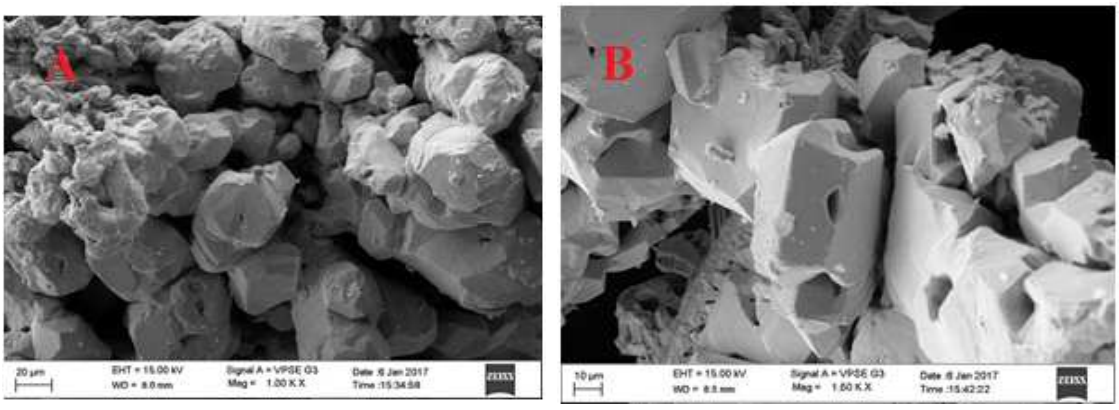

Figure 5: SEM Images of Electrochemically Synthesized In_2S_3 Nanoparticles

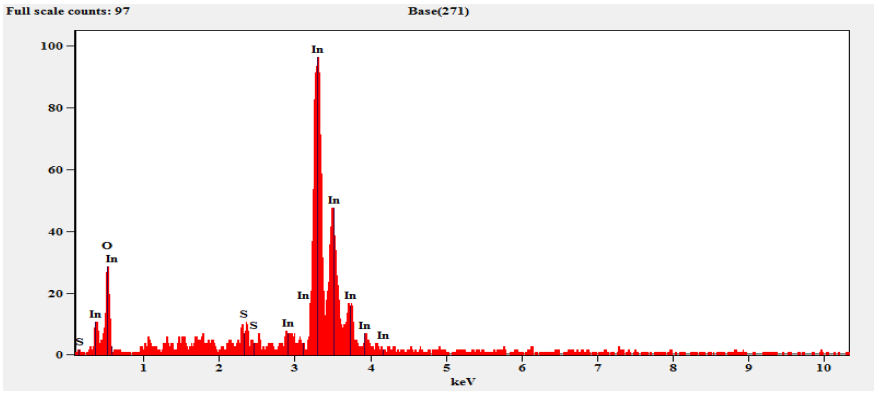

Figure 6: Energy Dispersive X-Ray Analysis Spectrum of In_2S_3 Nanoparticles

Transmission Electron Microscopy

The size and morphology of the synthesized In_2S_3 nanoparticles were investigated, using TEM. The TEM micrographs of cubic In_2S_3 showed that, the material is particulate (Figure7). The TEM images represented by figures 7(A) and 7(B) demonstrates that, obtained products have diameters 20 nm and 100 nm. The SEAD pattern as well as HRTEM observation provides additional insight, into the structure of cubic In_2S_3. From the XRD data, the average crystallite size calculated was 76.3nm, which is also corroborated by TEM.

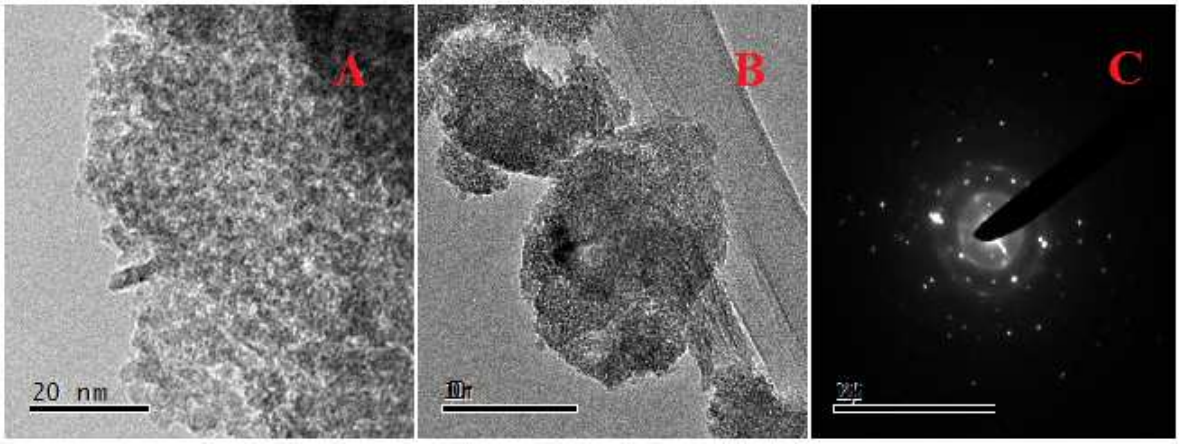

Figure 7: TEM Micrographs of In_2S_3 Nanoparticles

Measurement of Zeta Potential by Dynamic Light Scattering (DLS)

The Zeta potential of In_2S_3 nanoparticles were determined using Zeta sizer Nano-ZS90 (Malvern instruments). The analysis was performed at an angle of 90^0, at a temperature of 25^0C, using sample diluted with acetone at pH 7. The lower Zeta potential value In_2S_3 nanoparticle (Table 1) suggests that, the nanoparticles obtained from electrochemical method have a better stability of dispersion in aqueous solution, at neutral pH and can enhance the adsorption of cationic organics, on the surface and thus, improve the photo catalytic efficiency of cationic organic pollutants. The high conductivity and field strength of 4uS/cm and 5.0kV/m, respectively make In_2S_3 nanoparticle, a promising electronic applicant.

Table 1: Measurement of Zeta Potential of In_2S_3 Nanoparticles using DLS

Zeta Potential - ζ	
Mobility	0.01 u / S / V/ cm
Zeta potential	0.1 mV
Charge	0.00056 fC
Polarity	Positive
Conductivity	4 uS / cm
Field strength	5.0 kV/ m

Impedance Studies

The impedance analysis was performed in a frequency range, from 100 Hz to 10 K Hz, using WAYNE KERR 6500B precision impedance analyzer at room temperature. The Figure 8, shows the Bode plot [46] (variation of total impedance with frequency), for In_2S_3 nanoparticles. The total impedance values are typically lower at low frequency region and increases gradually with increasing frequency. After reaching a maximum, the impedance changes randomly, with respect to increase in frequency. The impedance study clearly indicates that, synthesized In_2S_3 nanoparticles are semiconductor photo catalysts.

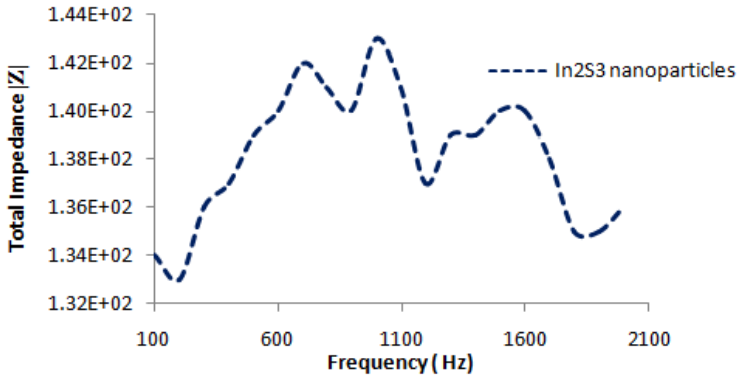

Figure 8: Bode Plot of Nano In_2S_3

PHOTOCATALYTIC DEGRADATION OF INDIGO CARMINE DYE AND COD MEASUREMENTS

Effect of Concentration of Indigo Carmine Dye

To ensure the optimum dye concentration, photodegradation is carried out with different concentration of Indigo carmine, with constant weight of catalyst. The change in the concentration of Indigo carmine, was recorded by change in colour using UV-Vis Spectrophotometer 117, Systronics. A plot of log% T verses time was linear, upto 60 % of the reaction indicating the disappearance of IC follows first order kinetics (Figure 9). The rate constant values are tabulated and the reaction rate decreases with increase in the dye concentration (Table 2). Beyond the optimum dye concentration, as the initial concentration of dye increases, the degradation efficiency reduces. The possible reason is that, as initial concentration of dye is increased, more dye molecules are adsorbed onto the surface of the catalyst. But, the adsorbed dye molecules are not degraded immediately, because the intensity of the light and the amount of catalyst is constant and also, the light penetration will be less. Also, with increase in dye concentration, the solution becomes more intense coloured and the path length of the photons entering the solution is decreased thereby, fewer photons reached the catalyst surface [38]. Hence, there will be reduction in the production of ROS species like hydroxyl and superoxide radicals [47]. Therefore, the photo degradation efficiency is reduced. The COD for IC solutions before and after degradation were measured and tabulated in Table 2.

Effect of Catalyst Loading

The experiments were performed by taking different amount of catalyst, varrying from 0.02 to 0.06g, in order to study the effect of catalyst loading (Figure 10 and table 2). Several studies have indicated that, photocatalytic rate initially increases with catalyst loading and then, decreases at high values because of light scattering and screening effects [38,48]. The tendency toward agglomeration also increases at high solid concentration, resulting in a reduction in the surface area available for light absorption and a decrease in photocatalytic degradation rate. The number of active sites in solution will increase with catalyst loading, a point appears to be reached, where light penetration is compromised because of excessive particle concentration [49]. A further increase in catalyst loading beyond the optimum (0.02g), will result in non- uniform light intensity distribution, so that, the reaction rate would indeed be lower with increased catalyst dosage.

Effect of pH

The pH of the solution is one of the important factors, in evaluating the photo degradation reaction in aqueous medium. In the present work, the pH of the solution was adjusted by adding 0.01M HCl solution and 0.01M NaOH

solution. The effect of pH was studied at pH 4, pH 6, pH 8 and pH 10, keeping all other experimental conditions constant. The results are illustrated in Figure 11 and tabulated in Table 2. It can be suggested that, the influence of pH on photo degradation is due to the amount of dye adsorbed on nanoparticles. It was observed that, the rate of photo catalytic degradation of IC increases, with increase in pH up to 10. This observation can be explained, on the basis that, as the pH of the solution increases, more OH^- ions are available. These OH^- ions will generate more OH radicals, by combining with the positive holes of the semiconductor [50]. These hydroxyl radicals are responsible for the degradation of the dye.

Re-Use of Photo Catalyst

The possibility of reusing the photocatalyst was examined to see the cost effectiveness of the method used (Figure 12 and table 2). After degradation of the dye, the dye solution was kept standing for 10 hrs and then, the supernatant liquid was decanted. The photocatalyst was thoroughly washed with double distilled water and then, reused for the photodegradation, by taking fresh IC dye solution. The re-use sample has shown almost same degradation efficiency compared to the fresh samples, while an obviously decrease in photoactivity was noticed with the reuse cycles [51]. This indicates the nano samples, that can be regenerated and re-used with slightly less efficiency. An obviously decrease in rate of reaction was observed, with the second use of catalyst. Reuse cycles might cause the aggregation of photocatalyst and the decrease in specific surface area and the losses of catalyst, resulting in a loss of catalytic activity [52].

Table 2: Effect of Different Variables on the Rate of Photodegradation of Indigo Carmine Dye

Variation	Amount of Catalyst(g)/Dye(M)	k sec^{-1}	Time Taken for Complete Degradation(min)	COD Values in mg/L		Degradation Efficiency %
				Before Degradation	After Degradation	
Concentration of dye	0.1×10^{-4} M	4.91×10^{-5}	210	304	32	89.47
	0.2×10^{-4} M	5.75×10^{-5}	250	352	16	95.45
	0.3×10^{-4} M	4.31×10^{-5}	410	360	64	82.82
Amount of catalyst	0.02g	5.75×10^{-5}	250	352	16	95.45
	0.04g	4.79×10^{-5}	310	352	32	90.90
	0.06g	4.68×10^{-5}	360	352	32	90.90
pH 4.0	0.2×10^{-4} M	4.24×10^{-5}	340	352	32	90.90
6.0	0.2×10^{-4} M	4.79×10^{-5}	330	352	32	90.90
8.0	0.2×10^{-4} M	6.97×10^{-5}	280	352	16	95.45
10.0	0.2×10^{-4} M	14.58×10^{-5}	135	352	16	95.45
Reuse of catalyst	0.2×10^{-4} M	3.59×10^{-5}	400	352	48	86.36

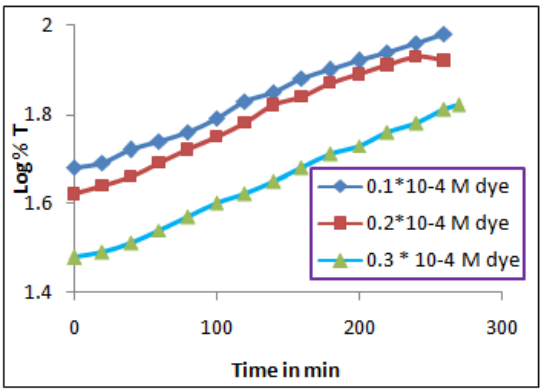

(a)

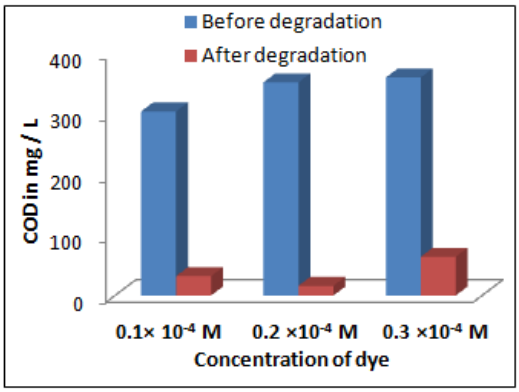

(b)

Figure 9: Plot of Log %T Vs Time for Different Initial Concentration of Dye (a) and the Effect of COD upon Degradation (b)

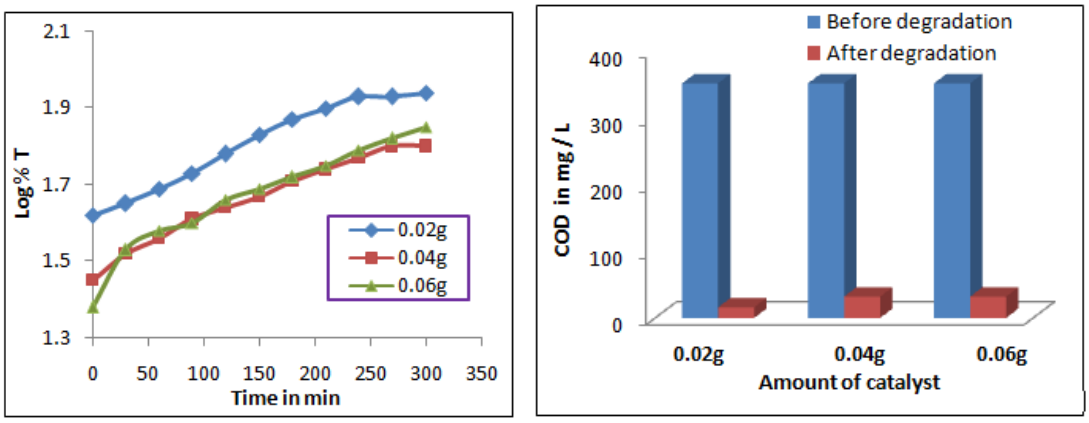

(a) **(b)**

Figure 10: Plot of Log %T Vs Time for Different Amounts of Catalyst (a) and the Effect of COD upon Degradation (b)

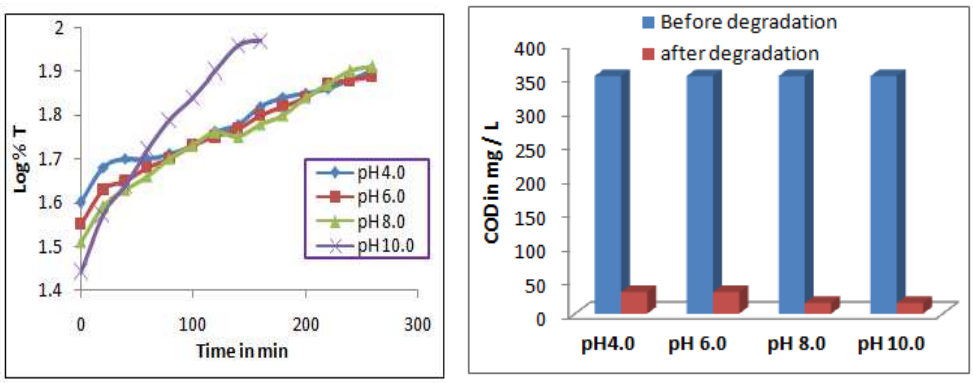

(a) **(b)**

Figure 11: Plot of Log % T Vs Time for Different pH of the Dye (a), and the Effect of COD upon Degradation (b)

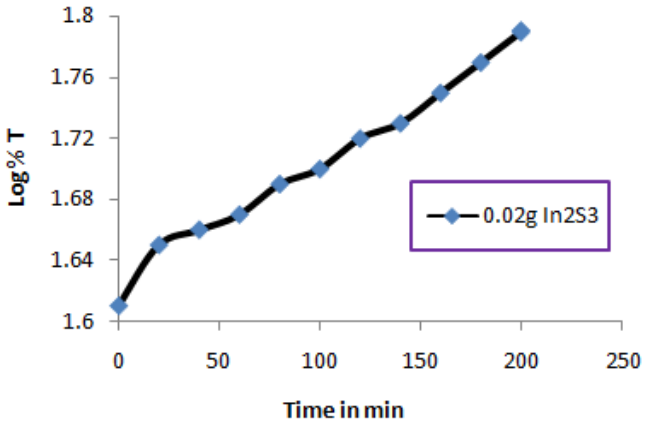

Figure 12: Plot of Log %T Vs Time for Reuse of Catalyst

BIOLOGICAL ACTIVITY

Antibacterial Activity

Bacterial Growth Condition

The Gram negative bioluminescent *Photo bacterium lieognathi* **(**accession number: KM434234), isolated from coastal area of Goa, were used in this study. Bacteria were grown in nutrient broth (NB) containing 3% sodium chloride, with aeration at 25˚C for 24 h. 10µl of the overnight culture was inoculated into 100 ml of nutrient broth and incubated under the same condition until the OD_{600} reaches 0.5 (approximately 12 hours), as at this OD bacteria were emitting the maximum amount of light.

Reagents

1mg/ml stock solution of nanoparticles was prepared in sterile distilled water. To disperse the nanoparticles, the suspension was sonicated, before use. Later, nanoparticles dilutions were prepared in sterile broth. As these solutions are later inoculated with an equal amount of bacteria in broth, the dilutions are prepared at concentration twice the desired final concentration.

Minimum Inhibitory Concentration (MIC) Assay

Broth microdilution technique has been used to determine the MIC of nanoparticle. For this purpose, two fold serial dilutions of the compound ranging from 500 to 0.4 mg/ml were performed in 96-well white microtiter plate. Initially 100 µl of bacterial inoculums was placed into the wells of the plate and later each well seeded with 100 µl of nanoparticle dilutions. Bacterial luminescent intensity was measured, using a luminometer (Varioskan ^{TM} Flash Multimode Reader, Thermo Scientific) after 6 hrs of incubation at 25˚C with 150 rpm shaking. In addition to the nanoparticle-treated well, each plate had untreated bacterial culture as control. Sterile broth containing nanoparticle and sterile broth, also served as blank for the test and control, respectively. Nanoparticle efficacy was calculated from the blanks, control and treated luminescence values on a plate:

Percentage of inhibition= $[(C-B_1)-(T-B_2)/(C-B_1)]*100$

where

B_1, B_2, C and T denotes the average luminescence of sterile broth, sterile broth containing nanoparticle, control and treated wells, respectively.

RESULT AND DISCUSSIONS

The % inhibition of bacterial growth at different concentrations of nanoparticles, is tabulated in table 3 and the results are plotted in figure 13. The MIC is defined as the lowest concentration of nanoparticles, that inhibits the growth of a microorganism. The percentage of inhibition for the nanoparticle has showed in table 3. The MIC value for the tested nanoparticle is 31.25 µg/ ml.

Table 3 Inhibition of Bacterial Growth at Different Concentrations of Nanoparticles (µg/ ml)

Nanoparticle Concentration (µg/ml)	500	250	125	62.5	31.25	15.6	7.8	3.9	1.9	0.97	0.48
% of Inhibition	142	127	125	118	100	89	81	77	74	70	20

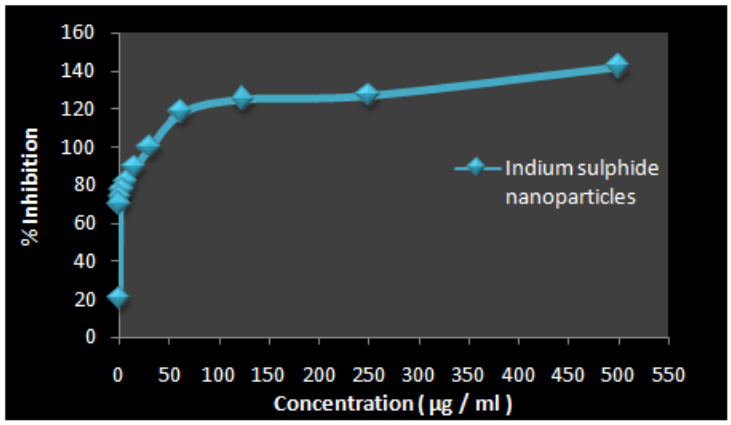

Figure 13: Plot of % Inhibition of Bacterial Growth V/s Concentration of Nanoparticle in µg/ ml

Antimitotic Activity

The antimitotic activities of synthesized naoparticles were determined by *Allium* assay method. *Allium cepa* has been used, to evaluate the antimitotic activity of synthesized Indium sulphide nanoparticles. The results of antimitotic activity are given in table 4 and percentage inhibition of cell division, by In2S3 nanoparticles compared to control is given in figure 14. The treatment of *Allium Cepa* cells with different concentrations of nanoparticles (25, 50 and 75 ppm), at different time duration (12, 18 and 24 hrs) exhibited changes in chromosomes and shape of the cells. The change in chromosomes and cellular morphology were achieved in increasing time and concentration. The synthesized Indium sulphide nanoparticles show good inhibitory effect, at 24hrs of treatment and acts as potent antimitotic agents.

Table 4: Antimitotic Activity Results of Indium Sulphide Nanoparticles by *Allium Cepa* Assay Method

Compound	Conc. in ppm	% Dividing Cells			% Dividing Cells Compared to Control			% Inhibition Compared to Control		
		12 hrs	18 hrs	24 hrs	12 hrs	18 hrs	24 hrs	12 hrs	18 hrs	24 hrs
Control	SDW	24.05	24.50	23.42	0.00	0.00	0.00	0.00	0.00	0.00
In_2S_3 nanoparticles	25	25.81	28.00	20.13	83.18	72.68	38.57	16.82	27.32	61.43
	50	31.64	33.15	17.34	69.82	62.42	25.99	30.18	37.58	74.01
	75	32.30	27.91	13.89	63.14	48.66	18.02	36.86	51.34	81.98

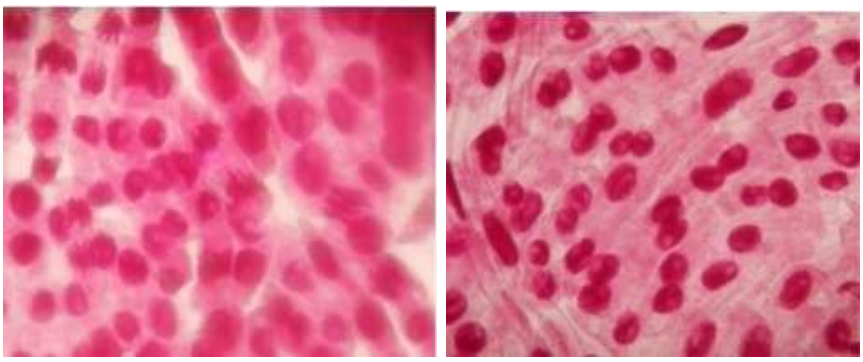

(A) (B)

Figure 14: Cell Growth Inhibitions by (A) Control and (B) In_2S_3 Nanoparticles

CONCLUSIONS

Cubic In_2S_3 nanoparticles were synthesized by electrochemical method, which is simple, cost effective and eco-friendly method. The photodegradation by this semiconductor offers a green technology, for removal of hazardous components (organic dyes) present in waste water and industrial effluents. Kinetics of photo-degradation of Indigo carmine suggested that, disappearance of IC follows first order kinetics and nanoparticles can be regenerated, and reused with slightly lesser efficiency. The complete degradation reaction was confirmed, by conducting COD experiment.

The synthesized nanoparticles are capable of entering into the bacterial cell and *Allium cepa* cell, therefore inhibits the cell growth and hence, confirms the biological activity, as a potent antibacterial and antimitotic agents.

ACKNOWLEDGEMENT

This work has been supported by University of Mysore, Mysore and the author Uma. H. B is thankful to UGC, New Delhi, for providing financial assistance through BSR meritorious fellowship.

REFERENCES

1. *J. Sterner, J. Malmstrom, L. Stolt (2005). Study on ALD In_2S_3 Cu(In, Ga)Se_2 interface formation. Progress in Photovoltaics, 13(3), 179-193.*
2. *Taneo Nishino, Yoshihiro Hamakawa (1977). Preparation and properties of InS single crystals. Japanese Journal of applied physics, 16 (8), 1291-1300*
3. *R. Jayakrishnan, Teny Theresa John, C. Sudha Kartha, K. P. Vijayakumar, T. Abe, Y. Kashiwab (2005). Defect analysis of sprayed β-In_2S_3 thin films using photoluminescence studies. Semiconductor Science and technology, 20 (12), 1162-1167*
4. *S. YuAB, L. ShuA, Y. QianAB, Y. XieAB, J. YangA, L. YangB (1998). Hydrothermal preparation and characterization of nanocrystalline powder of β-Indium sulphide. Materials research bulletin, 33(5), 717-721.*
5. *N. Kamoun, S. Belgacem, M. Amlouk, R. Bennaceur, J. Bonnet, F. Touhari, M .Nouaoura, L.Lassabatere (2001). Structure, surface composition and electrical properties of β-In_2S_3 and β- $In_{2-x}Al_xS_3$ Journal of applied physics, 89(5), 2766-2771*
6. *Sung-Hyu Choe, Tae-Hwan Bang, Nam-Oh Kim, Hyung-Gon Kim, Choong-II Lee, Moon-Seon Jin, Seok-Kyun Oh, Wha-Tek Kim (2001). Optical properties of β-In_2S_3 and β-In_2S_3:Co^{2+} single crystals. Semiconductor science and technology, 16 (2), 98-102*
7. *Wha-Tek Kim, Chang-Dae kim (1986). Optical energy gaps of β-In_2S_3 thin films grown by spray pyrolysis. Journal of applied physics, 60, 2631-2633.*
8. *Yoichi Yasaki, Noriyuki Sonoyama, Tadayoshi Sakata (1999). Semiconductor sensitization of colloidal In_2S_3 on wide gap semiconductors Journal of Electro analytical chemistry, 469 (2), 116-122*
9. *J.George, K.S.Joseph, B. Pradeep, T. I. Palson (1988). Reactively evaporated films of indium sulphide Physica Status Solidi A, 106 (1), 123-131*
10. *E. Dalas, S. Sakkopoulos, E. Vitoratos, G. Maroulis, L. Kobotiatis (1993). Aqueous precipitation and electrical properties of indium (III) sulphide: characterization of the indium (III) sulfide/ polyaniline andindium (III) sulfide/polypyrrole heterojunctions. Journal of material science, 28 (20), 5456-60*
11. *E. Dalas, L. Kobotiatis (1993). Primary solid state batteries constructed from copper and indium sulphides. Journal of Material Science, 28 (24), 6595-6597.*

12. A. Kudo, A. Nagane, I. Tsuji, H. Kato (2002). H_2 evolution from aqueous potassium sulfite solutions under visible light irradiation over a novel sulfide photocatalyst $NaInS_2$ with a layered structure Chemistry letters, 31 (9), 882-883

13. S. D. Naik, T. C. Jagadale, S. K. Apte, S. Sonawane, M. V. Kulkarni, S. I. Patil, S. B. Ogale, B. B. Kale (2008). Rapid phase-controlled microwave synthesis of nanostructured hierarchical tetragonal and cubic β-In_2S_3 dandelion flowers Chemical physics letters, 452 (4-6), 301-305

14. Frank E. Osterloh (2008). Inorganic materials as catalysts for photochemical splitting of water.Chemistry of Materials, 20(1), 35-54

15. Xianliang Fu, Xuxu Wang, Zhixin Chen, Zizhong Zhang, Zhaohui Li, Dennis Y.C.Leung, Ling Wu, Xianzhi Fu (2010). Photocatalytic performance of tetragonal and cubic β-In_2S_3 for the water splitting under visible light irradiation Applied Catalysis B: Environmental, 95(3-4), 393- 399.

16. Dattatri K.Nagesha, Xiaorong Liang, Arif.A.Mamedov, Gordon Gainer, Margaret A.Eastman, Micahel Giersig, Jin-Joo Song, Tong Ni, Nicholas A.Kotov (2001). In_2S_3 nanocolloids with excitonic emission: In_2S_3 vs CdS comparative study of optical and structural characteristics. Journal Physical Chemistry B, 105 (31), 7490-7498.

17. Weimin Du, Jun Zhu, Shixiong Li, Xuefeng Qian (2008).Ultrathin β-In_2S_3 nanobelts: shape-controlled synthesis and optical and photocatalytic properties. Crystal Growth & Design, 8 (7), 2130-2136.

18. Yunhui He, Danzhen Li, Guangcan Xiao, Wei Chen, Yibin Chen, Meng Sun, Hanjie Huang, Xianzhi Fu (2009). A new application of nanocrystal In_2S_3 in efficient degradation of organic pollutants under visible light irradiation The Journal of Physical Chemistry C, 113(13), 5254- 5262

19. R.Kumaresan, M.Ichimura, N.Sato, P.Ramasamy (2002). Application of novel photochemical deposition technique for the deposition of indium sulphide Material science and engineering: B, 96(1), 37- 42.

20. R.S. Mane, C.D. Lokhande (2002). Studies on structural, optical and electrical properties of indium sulfide thin films. Materials Chemistry and Physics, 78 (1), 15-17.

21. N.Barreau, S.Marsillac, J.C.Bernede, T.B.Nasrallah, S.Belgacem (2001). Optical properties of wide band gap indium sulphide thin films obtained by physical vapor deposition. Physics Status Solidi A, 184 (1), 179-186.

22. Hongjie Dai, Eric W.Wong, Charles M.Lieber (1996). Probing electrical transport in nanomaterials: conductivity of individual carbon nanotubes. Science, 272 (5261), 523-526.

23. Xie Y, Qian Y, Wang W, Zhang S, Zhang Y (1996). A benzene- thermal synthetic route to nanocrystalline GaN. Science, 272 (5270), 1926-1927.

24. C.B.Murry, D.J.Norris, M.G.Bawendi (1993). Synthesis and characterization of nearly monodisperse CdE (E= sulfur, selenium, tellurium) semiconductor nanocrystallites. Journal of the American Chemical Society, 115 (19), 8706-8715.

25. L.Brus (1991).Quantum crystallites and non linear optic., Applied Physics A, 53(6), 465-474.

26. N.Naghavi, S.Spiering, M.Powalla, B.Cavana, D.Lincot (2003). High-efficiency copper indium gallium diselenide (CIGC) solar cells with indium sulphide buffer layers deposited by atomic layer chemical vapor deposition (ALCVD). Progress in Photovoltaics: Research and applications, 11(7), 437-443.

27. Yujie Xiong, Yi Xie, Guong Du, Xiaobo Tian, Yitai Qian (2002). A novel in situ oxidation-sulfidation growth route via self-purification process to β-In_2S_3 dendrites. Journal of Solid State Chemistry, 166 (2), 336-340.

28. Mohammmad Afzaal, Mohammad A.Malik, Paul O' Brien (2004). Indium sulphide nanorods from single-source precursor. Chemical Communications, 3, 334-335.

29. *Yujie Xiong, Yi Xie, Guong Du, Xiaobo Tian (2002). A solvent-reduction and surface modification technique to morphology control of tetragonal In_2S_3 nanocrystals. Journal of Material Chemistry,12 (1), 98-102.*
30. *S.Avivi, O.Palchik, V.Palchik, M.A.Slifkin, A.M.Weiss, A.Gedanken (2001). Sonochemical synthesis of nanophase indium sulphide. Chemistry of Materials, 13 (6), 2195-2200.*
31. *Won-Kyu Han, Jae-Woong Choi, Gil- Ho Hwang, Seok – Jun Hong, Jai-Sung Lee, Sung Goon Kang (2006). Fabrication of Cu nano particles by direct electrochemical reduction from CuO nano particles. Applied Surface Science, 252(8), 2832-2838.*
32. *L.Rodri´guez – Sa´nchez, M.C.Blanco, M.A.Lo´pez-Quintela (2000). Electrochemical synthesis of silver nanoparticles. Journal of Physical Chemistry B, 104 (41), 9683-9688.*
33. *CheonhoYoon, Jung Sang Suh (2002). Electrochemical fabricationof CdS/Co nanowire arrays in porous aluminium oxide templates. Bull. Korean Chem.Soc, 23 (11), 1519-1523.*
34. *O.Vazquez- Cuchillo, R.Gomez, A.Cruz- Lopez, L.M.Torres- Martinez, R.Zanella, F.J.Alejandre Sandoval, K.Del Angel-Sanchez (2013).Improving water splitting using RuO_2-Zr / $Na_2Ti_6O_{13}$ as a photocatalys., Journal of Photochemistry and Photobiology A: Chemistry, 266, 6-11.*
35. *C.Coudray, S.Rachidi, A.Favier (1993). Effect of Zinc on superoxide – dependent hydroxyl radical production in vitro. Biological Trace Element Research, 38, 273-287.*
36. *G.Chaitanya Lakshmi, S.Ananda, R.Somashekar, C.Ranganathaiah (2012). Synthesis of ZnO / ZrO_2 Nano Composites by electrochemical method and its application for photocatalytic degradation of Fast Green FCF Dye and paper dyeing and printing press effluents. International journal of Advanced Materials Sciences, 3, 221-237.*
37. *K.Byrappa, A.K.Subramani, S.Ananda, K.M.Lokanatha Rai, R.Dinesh, M.Yashimura (2006). Photocatalytic degradation of rhodamine B dye using hydrothermally synthesized ZnO. Bulletin of Materials Science, 29 (5), 433-438.*
38. *A.K.Subramani, K.Byrappa, S.Ananda, K.M.Lokanatha Rai, C.Ranganathaiah, M.Yashimura (2007). Photocatalytic degradation of Indigo Carmine dye using TiO_2 impregnated activated Carbon. Bulletin of Materials Science, 30 (1), 37- 41.*
39. *N.Neelakandeswari, G.Sangami, N.Dharmaraj, Nam Ki Taek, Hak Yong Kim (2011). Spectroscopic Investigations on the photodegradation of Toluidine Blue dye using Cadmium sulphide nanoparticles prepared by a novel Method. Spectrochimica Acta Part A, 78 (5), 1592- 1598.*
40. *Ying Xue, Qingfen Luan, Dan Yang, Xin Yao, Kebin Zhou (2011). Direct evidence for hydroxyl radical scavenging activity of Cerium Oxide nanoparticles. The Journal of Physical Chemistry, 115 (11), 4433-4438.*
41. *S.H.Mohamed, (2010).Photocatalytic, Optical and electrical properties of Copper doped Zinc Sulfide thin films. Journal of Physics D: Applied Physics, 43, Article ID: 035406.*
42. *Yi Liu, Meng Zhang, Yongqian Gao, Rui Zhang, Yitai Qian (2007). Synthesis and optical properties of cubic In_2S_3 hollow nanospheres. Materials chemistry and physics, 101(2-3), 362-366.*
43. *Chengfang Li, Gongwu Song (2009). Photocatalytic degradation of organic pollutants and detection of chemical oxygen demand fluorescence method. Sensors and Actuators B: Chemical, 137 (2), 432-436.*
44. *G.Chaitanya Lakshmi, S.Ananda, R.Somashekar, C.Ranganathiah (2012). Synthesis, characterization and photocatalytic activity of ZnO:Sn nanocomposites. International Journal of Advances Science and Technology, 5, 54-64.*
45. *Sudip K. Batabyal, Shu En Lu, Jagadese J. Vittal (2016). Synthesis, characterization, and photocatalytic properties of In_2S_3, $ZnIn_2S_4$, and $CdIn_2S_4$ nanocrystals. Crystal Growth and Design,16 (4), 2231-2238.*

46. *K.R.Raksha and Sannaiah Ananda (2014). An investigation on kinetics of photocatalysis, electrical property and biological activity of electrochemically synthesized ZnS and Ru: ZnS nsanophotocatalysts. Journal of Applicable Chemistry, 3 (1), 397-412.*

47. *Wenjuan Li, Danzhen Li, Jinxiu Wang, Yu Shao, JinmaoYou, Fei Teng (2013). Exploration of the active species in the photocatalytic degradation of Methyl Orange under UV light irradiation. Journal of Molecular Catalysis A: Chemical, 380, 10-17.*

48. *Li HQ, Hong WS, Cui YM, Jia, QF, Fan SH (2013). High photocatalytic activity of C-ZnSn $(OH)_6$ catalysts prepared by hydrothermal method. Journal of Molecular Catalysis A: Chemical, 378, 164-173.*

49. *Nesic Jelena., Manojlovic Dragan D, Andelkovic Ivan, Dojcinovic, Biljana P, Vulic Predrag J, Krstic Jugoslav, Roglic Goran M (2013). Preparation, characterization and photocatalytic activity of Lanthanum and Vanadium Co-doped mesoporous TiO_2 for Azo-Dye degradation. Journal of Molecular Catalysis A: Chemical, 378, 67-75.*

50. *Babak Kaboudin, Foad Kazemi, Abolfazl Ghaderian, Ehsan Navidi, Zahra Zand (2014). A novel method for the synthesis of Fe_3O_4 nanoparticles/CdS nanowires heterostructure nanocomposite and uses in photodegradation of methylene blue. Journal of sulfur Chemistry, 35 (3), 279-289.*

51. *W.I.Nawawi, and M.A.Nawi (2014). Carbon coated Nitrogen doped P25 for the photocatalytic removal of Organic pollutants under solar and low energy visible light irradiations. Journal of Molecular Catalysis A: Chemical, 383-384, 83-93.*

52. *Wan-Jun Sun, Jun Li, Giuseppe Mele, Zeng-Qi Zhang, Feng -Xing Zhang (2013). Enhanced photocatalytic degradation of Rhodamine B by surface modification of ZnO with Copper (II) Porphyrin under both UV-Vis and Visible light irradiation. Journal of Molecular Catalysis A: Chemical, 366, 84-91.*